



**HAL**  
open science

## A damage model for volcanic edifices: Implications for edifice strength, magma pressure, and eruptive processes

Aurore Carrier, Jean-Luc Got, Aline Peltier, Valérie Ferrazzini, Thomas Staudacher, Philippe Kowalski, Patrice Boissier

### ► To cite this version:

Aurore Carrier, Jean-Luc Got, Aline Peltier, Valérie Ferrazzini, Thomas Staudacher, et al.. A damage model for volcanic edifices: Implications for edifice strength, magma pressure, and eruptive processes. *Journal of Geophysical Research : Solid Earth*, 2015, 120, pp.567-583. 10.1002/2014JB011485 . insu-03580033

**HAL Id: insu-03580033**

**<https://insu.hal.science/insu-03580033>**

Submitted on 18 Feb 2022

**HAL** is a multi-disciplinary open access archive for the deposit and dissemination of scientific research documents, whether they are published or not. The documents may come from teaching and research institutions in France or abroad, or from public or private research centers.

L'archive ouverte pluridisciplinaire **HAL**, est destinée au dépôt et à la diffusion de documents scientifiques de niveau recherche, publiés ou non, émanant des établissements d'enseignement et de recherche français ou étrangers, des laboratoires publics ou privés.

Copyright

## RESEARCH ARTICLE

10.1002/2014JB011485

## Special Section:

Stress, Strain and Mass  
Changes at Volcanoes

## Key Points:

- Preeruptive accelerations of surface displacement at PdF volcano are explained by the damage of the edifice under the action of a pressurized magma reservoir
- Magma reservoir pressure may decrease when damage increases and surface displacement accelerates
- Rock strength may be modeled at the scale of the edifice by this approach

## Correspondence to:

J.-L. Got,  
jlgot@univ-savoie.fr

## Citation:

Carrier, A., J.-L. Got, A. Peltier, V. Ferrazzini, T. Staudacher, P. Kowalski, and P. Boissier (2015), A damage model for volcanic edifices: Implications for edifice strength, magma pressure, and eruptive processes, *J. Geophys. Res. Solid Earth*, 120, 567–583, doi:10.1002/2014JB011485.

Received 24 JUL 2014

Accepted 7 DEC 2014

Accepted article online 11 DEC 2014

Published online 18 JAN 2015

## A damage model for volcanic edifices: Implications for edifice strength, magma pressure, and eruptive processes

Aurore Carrier<sup>1,2</sup>, Jean-Luc Got<sup>1,2</sup>, Aline Peltier<sup>3,4</sup>, Valérie Ferrazzini<sup>3,4</sup>,  
Thomas Staudacher<sup>3,4</sup>, Philippe Kowalski<sup>3,4</sup>, and Patrice Boissier<sup>3,4</sup>

<sup>1</sup>Université de Savoie, ISTerre, Le Bourget-du-Lac, France, <sup>2</sup>CNRS, ISTerre, Le Bourget-du-Lac, France, <sup>3</sup>Institut de Physique du Globe de Paris et Université Paris-Diderot, Paris, France, <sup>4</sup>Observatoire Volcanologique du Piton de la Fournaise, IPGP, CNRS, La Plaine des Cafres, France

**Abstract** Monitoring of large basaltic volcanoes, such as Piton de la Fournaise (La Réunion Island, France), has revealed preeruptive accelerations in surface displacements and seismicity rate over a period of between 1 h and several weeks before magma reaches the surface. Such eruptions are attributed to ruptures of pressurized magma reservoirs. Elastic models used to describe surface deformation would assume that accelerations in surface deformation are due to increases in reservoir pressure. This assumption requires changes in magma or pressure conditions at the base of the magma feeding system that are unrealistic over the observed timescale. Another possible cause for these accelerations is magma pressure in the reservoir weakening the volcanic edifice. In the present study, we modeled such weakening by progressive damage to an initially elastic edifice. We used an incremental damage model, with seismicity as a damage variable with daily increments. Elastic moduli decrease linearly with each damage increment. Applied to an initially elastic edifice with constant pressure at the base of the system, this damage model reproduces surface displacement accelerations quite well when damage is sufficient. Process dynamics is controlled by the damage parameter, taken as the ratio between the incremental rupture surface and the surface to be ruptured. In this case, edifice strength and magma reservoir pressure decrease with decreasing elastic moduli, whereas surface displacement accelerates. We discuss the consequences of pressure decreases in magma reservoirs.

### 1. Introduction

Many large basaltic volcanoes are now continuously monitored for surface deformation and seismicity. The resulting data suggest the existence of magma reservoirs and feeding systems in their edifices and reveal the main features of their dynamics [e.g., Peltier *et al.*, 2007; Bonforte *et al.*, 2008; Montgomery-Brown *et al.*, 2011]. Eruptions occur when the pressure in the magma reservoir reaches the strength of the edifice and provokes the rupture of the reservoir [Blake, 1984; Tait *et al.*, 1989; McLeod and Tait, 1999; Gudmundsson, 2006; Gerbault *et al.*, 2012]. Intereruptive and preeruptive changes in deformation and seismicity are common features of these volcanoes. The most frequent changes in geophysical observables are an increase in seismicity rate or in RSAM amplitude [Voight, 1988; Kilburn, 2003; Lengliné *et al.*, 2008; Schmid *et al.*, 2012; Budi-Santoso *et al.*, 2013]. In some cases, this increase is accompanied by an acceleration in surface deformation [see, e.g., Peltier *et al.*, 2005, 2006, 2009a; Surono *et al.*, 2012; Kilburn, 2012; see Schmid *et al.*, 2012 for a systematic study of this pattern on Piton de la Fournaise], whereas in other cases, surface deformation stabilizes for a period of time. Schmid *et al.* [2012] calculations of average seismicity and surface deformation rates for Piton de la Fournaise volcano between 1999 and 2006 clearly revealed an average acceleration pattern during intereruptive periods and a remarkable preeruptive dynamics with a very slow deformation pattern changing into a very fast deformation pattern in some days.

Lengliné *et al.* [2008] drew up an elastic modelling of a pressurized magma reservoir fed by a magma conduit in an elastic half-space, with a constant pressure condition at the base of the magma conduit. In such a case, the magma reservoir pressure may be expressed in a very simple analytical form which shows that due to the elastic nature of the volcanic edifice model, equilibrium is reached with a constant magma reservoir pressure and subsequent limited surface deformation. This occurs over a characteristic time period ranging from tens of days to 1 year, depending mostly on the geometry of the system and magma viscosity. Using such a model to explain surface deformation accelerations over time periods of days to tens of days would require a systematic analogue pressure change at the base of the conduit, in the mantle, once the

feeding system equilibrium is reached. Whether such an ad hoc mantle process is realistic at this timescale is questionable.

Accelerations in acoustic emission rates and deformation preceding rupture have long been observed during laboratory rock deformation experiments, at the sample scale. They are usually related to the progressive damage and rupture event interactions, termed tertiary creep, which occur before the final instability and failure [see, e.g., Cox and Meredith, 1993; Main, 2000; Amtrano and Helmstetter, 2006]. Cox and Meredith [1993] linked stress and strain in a damage model of the weakening behavior of progressively cracked elastic solids. Benson *et al.* [2007] imaged the complete slow failure process in triaxially deformed Etna basalt, monitoring accelerations in volume changes and acoustic emissions, and [Heap *et al.*, 2009, 2010] examined the decrease in elastic moduli due to damage in samples in volcanic rocks. At a larger scale, Agnon and Lyakhovskiy [1995] and Mériaux *et al.* [1999], respectively, evidenced and studied damage during dyke propagation. In a study of brittle creep in basalt under constant stress, based on measurements of axial strain, porosity, and acoustic emission energy, Heap *et al.* [2011] showed that creep could explain seismic activity and strain release recorded at Mount Etna between 1993 and 2005. Similar measurements have been made on other volcanoes [e.g., Ventura *et al.*, 2010], mostly in order to check the applicability of eruption prediction methods such as the Failure Forecast Method (FFM, Voight [1988]; see Tarraga *et al.* [2008] for a review, more recently Bell *et al.* [2011a, 2011b] for evaluations, and A. Boué *et al.* (Real-time eruption forecasting using the material Failure Forecast Method with a Bayesian approach, submitted to *Journal of Geophysical Research*, 2015)), which is derived from studies of tertiary creep and material failure under constant load. In studies investigating the possibility of using FFM to predict eruption, the damage variable may be the seismicity or the strain rate, and the applied stress has always been considered constant, which may not be the case.

However, seismicity rates and surface deformation records have never been used in large-scale physical models that use a damage approach to investigate how variations in applied stresses or pressures are linked to seismicity and deformation on volcanoes. In the present study, we used a progressive homogeneous isotropic damage approach in order to link seismicity to the progressive failure of rocks and to model the strain weakening of rocks and the subsequent acceleration of the deformation before failure. We first set up a reference model consisting of a pressurized magma reservoir embedded in a homogeneous isotropic elastic half-space and fed by a magma conduit with constant magma pressure at its base, similar to the model used in Lengliné *et al.* [2008]. Reservoir pressure time evolution is deduced from the fact that over a given time, magma volume input to the reservoir is equal to the change in reservoir volume, in the hypothesis that magma is incompressible and that no magma loss occurs. Damage was introduced into the model by a law that reduces the elastic shear modulus, using the seismicity rate as a damage variable and the characteristic rupture length as a damage parameter. We computed overpressure in the reservoir from the numerical integration of a nonlinear, first-order differential equation, and we deduced theoretical surface displacements from the reservoir overpressure as a function of time. We then used these surface displacements to fit the time evolution of the measured surface displacements, which constrained the evolution of the reservoir overpressure over time. Best fit was obtained by adjusting the characteristic rupture length in the damage law. This study allowed us to infer the prepeak stress-strain behavior on the scale of a volcanic edifice and to model the pressure history in the magma reservoir during interruptive and preeruptive periods. It is important to determine how reservoir pressure evolve over time, as this parameter controls the eruptive dynamics of volcanoes. The present study complements Got *et al.* [2013]'s study of the postpeak behavior of the volcanic edifice during distal eruptions of Piton de la Fournaise.

Our study was based on surface displacement data recorded from the permanent GPS station network operated by the Observatoire Volcanologique du Piton de la Fournaise (OVPF) in La Réunion Island (France). Piton de la Fournaise is an active hot spot shield volcano that erupted 35 times from 1998 to 2014, emitting more than  $500 \times 10^6 \text{ m}^3$  of magma [Roult *et al.*, 2012]. Seismic tomography [Nercessian *et al.*, 1996; Prôno *et al.*, 2009] and inversion of geodetic data [Peltier *et al.*, 2007, 2008, 2009b] indicate the presence of a shallow magma reservoir located between 0 m and 500 m above sea level. The volcanic edifice's stable western flank is separated from its mobile eastern flank by a rift system (see, e.g., Bachèlery [1981] and Michon *et al.* [2007]) that radiates from the eruptive center, located at the 1 km diameter Dolomieu crater (Figure 1). Geological observations on the Piton de la Fournaise and Piton des Neiges volcanoes show that most magma transfer occurs through subvertical dikes or subhorizontal sill injections in the volcanic edifice [Michon *et al.*, 2007; Letourneur *et al.*, 2008].

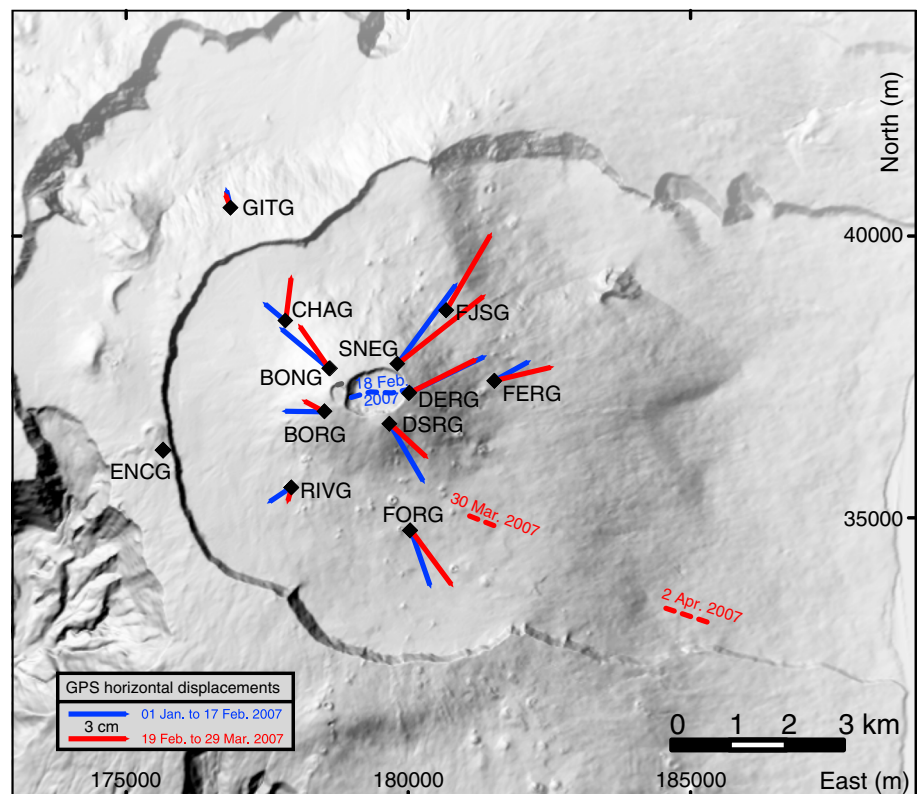


**Figure 1.** Digital elevation model of Piton de la Fournaise showing the location of the OPVF permanent GPS network (black diamonds). Vectors show horizontal displacements recorded during the two intereruptive periods investigated in this study: from 1 January 2007 to 17 February 2007 (blue) and from 19 February 2007 to 29 March 2007 (red). Dashed lines indicate the location of the eruptive fissures that opened on 18 February (blue) and 30 March and 2 April 2007 (red). Coordinates are given in the Gauss-Laborde Réunion projection system.

## 2. Data

### 2.1. Deformation Data

Because our aim was to model surface deformation on the volcano over short timescales (typically days to weeks), we used the daily surface displacement data recorded by the OPVF permanent GPS network (Figure 1). Our study focused on the 18–19 February and 30 March to 1 May 2007 eruptions (Figures 1 and 2), during which well-recorded eruptive activity occurred (see, e.g., *Staudacher et al.* [2009] and *Peltier et al.* [2009b]) for a more detailed description of these eruptions). In 2007, the network consisted of 10 GPS stations located around the summit of Piton de la Fournaise, with another two GPS stations approximately 4 km from the summit (Figure 1). GPS signals were recorded at a rate of 2 samples/min. Daily solutions were determined using the GAMIT/GLOBK software package, which takes into account IGS precise ephemeris, a stable support network of 20 IGS stations around La Réunion Island, a tested parameterization of the troposphere, a model of ocean loading, and solar and lunar tide models.

### 2.2. Seismicity Data

For the purposes of our study, we used the OPVF's catalogue of earthquakes at Piton de la Fournaise. OPVF has recorded continuous seismic data since March 1999, using a permanent seismic network which, until 2011, consisted of 15 stations operating short-period L4C seismometers and recording at a 100 Hz sampling frequency. The catalogue was established from continuous paper records (eight stations) by the OPVF staff and events classified as VT (volcanotectonic), RF (Rock Fall), or other types of earthquakes (local, regional, teleseism).

We used only VT earthquakes for our study. Most of these earthquakes occurred below the summit in a vertical, 1 km diameter cylinder at an elevation of between 0.5 and 1.5 km above sea level [*Massin et al.*, 2011] and above a superficial magma reservoir that has been shown to be above sea level from deformation

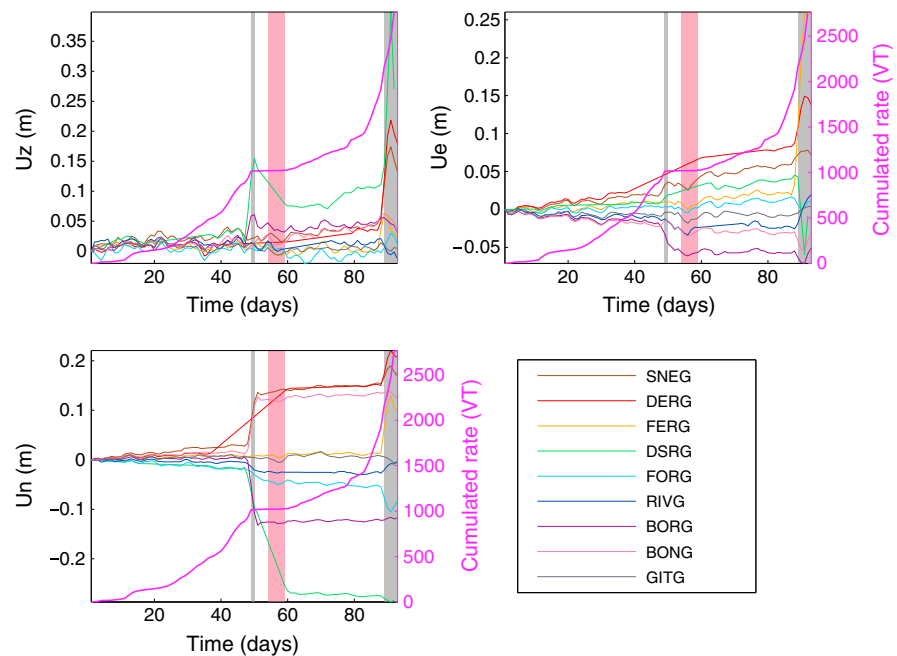


**Figure 2.** Cumulative seismicity in number of earthquakes (purple) and GPS displacement ( $U_z$ : vertical,  $U_e$ : East,  $U_n$ : North) as a function of time in days from 1 January 2007 to 3 April 2007 for various geodetic stations (see color correspondence in the inset) at Piton de la Fournaise volcano. Vertically shaded grey areas indicate the 18–19 February 2007 (left) and the beginning of the 30 March to 1 May 2007 eruptions. The vertically shaded pink area indicates the time during when the Gamède storm struck the island (23 to 28 February), when few data were acquired by the OVPF seismic network.

modeling [Peltier *et al.*, 2007] and seismic tomography [Prôno *et al.*, 2009]. Seismicity at Piton de la Fournaise mainly consists of low-magnitude earthquakes ( $M < 4$ ). Since 2002, magnitudes have been computed by OVPF as duration magnitudes, using the relation

$$M_d = 2 \log_{10} T + 0.0035\Delta - 0.87 \quad (1)$$

where  $T$  is the signal duration in seconds and  $\Delta$  is the epicentral distance in kilometer. Completion magnitude of the catalogue was computed using the maximum curvature method [Woessner and Wiemer, 2005] and found to be 0.3.

These seismic catalog and magnitude data can be used to infer the rupture area and the characteristic length for each earthquake, using the scaling relationships established by Wells and Coppersmith [1994]. Computation of the area ruptured by each of the ~55000 earthquakes that occurred between 1 January 2002 and 31 December 2011 showed that rupture length was roughly constant during this period (Figure 3). Characteristic rupture length is found to be ~66 m. This constant and small rupture length shows that stress transfer and earthquake interaction remained moderate, so small-magnitude earthquakes dominated the long-term rupture process.

### 3. Model

The following sections describe how we computed theoretical displacements at the surface of a volcanic edifice by using a simple model of a magma pressure source embedded in a damaged homogeneous elastic medium, using seismicity rate as a damage variable. Damage is introduced by decreasing the elastic moduli, following the linear isotropic approach of Kachanov [1958]. We considered magma to be a single-phase, incompressible fluid. This physical model was described by a nonlinear differential equation with magma reservoir overpressure as a variable, which we solved numerically. Theoretical surface displacements were inferred from the overpressure computation. Finally, model parameters were estimated by fitting the theoretical surface displacements to measured surface displacements.

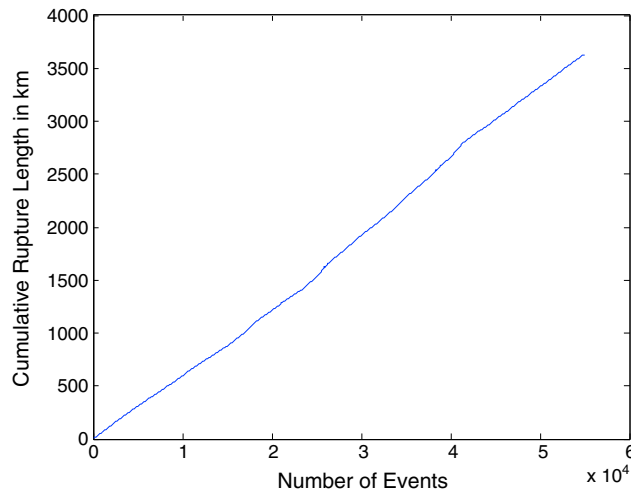


**Figure 3.** Cumulated rupture length in kilometer as a function of the number of volcanotectonic events between 1 January 2002 and 31 December 2011 at Piton de la Fournaise. Each rupture length was computed as the square root of the rupture area  $A$  deduced from the [Wells and Coppersmith, 1994] scaling law:  $A = 10^{-2.87+0.82*M}$ , where  $M$  is the local magnitude.

**3.1. Reference Elastic Model and Implications**

We built a 2-D axisymmetric model consisting of a pressurized spherical magma reservoir with constant source pressure at the base of a cylindrical magma conduit in a semiinfinite elastic half-space. This model is similar to the one published by *Lengliné et al.* [2008] (Figure 4). The magma reservoir has a radius  $a_r$ . It is fed by a conduit of length  $H_c$  and diameter  $a_c \ll a_r$ . Rising magma flow is laminar and Poiseuille’s law can be applied to the conduit:

$$Q = \frac{\pi a_c^4}{8\mu} \left( -\frac{dP}{dz} - \rho_m g \right) \quad (2)$$

where  $\frac{dP}{dz}$  is the vertical pressure gradient, and  $\mu$  and  $\rho_m$  are the magma viscosity and density, respectively. This can be written [Pinel and Jaupart, 2003]

$$Q(t) = \frac{\pi a_c^4}{8\mu H_c} (P - \Delta P(t)) \quad (3)$$

$P = \Delta P_s - \Delta P_r^0 + (\rho_r - \rho_m) g H_c$  is a constant term, where  $\Delta P_s$  is the overpressure at the source,  $\Delta P_r^0$  is the initial overpressure in the reservoir,  $\rho_r$  is the rock density.  $\Delta P_r(t) = \Delta P_r^0 + \Delta P(t)$  is the overpressure in the reservoir, and  $\Delta P(t)$  is the time history of the overpressure in the reservoir since the initial time.

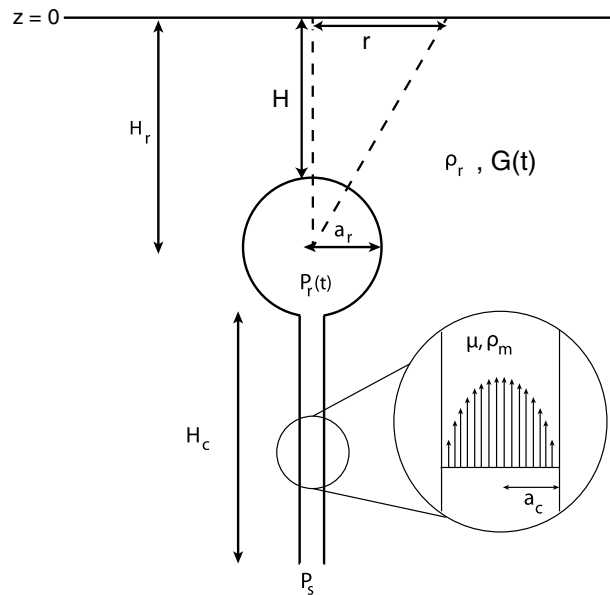


**Figure 4.** Physical model used in this study. A magma reservoir (radius  $a_r$ , depth  $H_r$ , roof depth  $H$ ) embedded in a semiinfinite homogeneous isotropic elastic half-space (density  $\rho_r$ , shear modulus  $G$ ) is fed by magma through a cylindrical conduit (radius  $a_c$ , length  $H_c$ ). Shear modulus  $G$  is assumed to change homogeneously with damage (see text for details) and therefore with time  $t$ . Pressure  $P_s$  at the base of the conduit is assumed to be constant. Magma is characterized by its viscosity  $\mu$  and its density  $\rho_m$ .

Writing volume variation into the magma reservoir without loss of magma [Delaney and McTigue, 1994] gives

$$\Delta V_{in}(t) = \Delta P(t) \frac{\pi a_r^3}{G} \quad (4)$$

where  $G$  is the shear or rigidity modulus and  $\Delta P(t)$  is the variation in the magma reservoir overpressure.

Considering that magma flow in the conduit is equal to the time derivative of the reservoir volume variation, we found the first-order differential equation [Lengliné et al., 2008]:

$$\frac{d\Delta P(t)}{dt} = \frac{G a_c^4}{8\mu H_c a_r^3} (P - \Delta P(t)) \quad (5)$$

Equation (5) has an analytical solution

$$\Delta P(t) = P \left( 1 - e^{-\frac{t}{\tau}} \right) \quad (6)$$

where  $\tau = \frac{8\mu H_c a_r^3}{G a_c^4}$  is the characteristic time of the overpressure function.

This simple elastic solution shows that when the pressure at the base of the magma conduit (the source) is constant, the magma reservoir reaches an equilibrium with a limit pressure controlled by the overpressure at the source.

If shear modulus  $G$  varies with time, time derivation of the volume variation (equation (4)) gives

$$\frac{d\Delta V_{in}(t)}{dt} = \frac{\pi a_r^3}{G(t)} \left( \frac{d\Delta P(t)}{dt} - \frac{\Delta P(t)}{G(t)} \frac{dG(t)}{dt} \right) \quad (7)$$

and equation (5) becomes

$$\frac{d\Delta P(t)}{dt} = \frac{G(t)a_c^4}{8\mu H_c a_r^3} (P - \Delta P(t)) + \frac{\Delta P(t)}{G(t)} \frac{dG(t)}{dt} \quad (8)$$

Equation (8) does not accept an analytical solution. Consequently, we computed  $\Delta P(t)$  numerically using a fourth-order Runge-Kutta scheme with a sixth-order adaptative step size control [Press, 1992]. In such a case, the solution may have a complex time evolution, depending on the time history of the shear modulus  $G$ . We defined a pseudo-characteristic time  $\tau^* = \frac{8\mu H_c a_c^4}{G(t)a_r^3}$  in order to represent the dynamics of the pressure time history.

Finally, we computed surface displacements, taking into account the free-surface effect, by using [Lisowski, 2007]

$$\begin{pmatrix} u_x \\ u_y \\ u_z \end{pmatrix} = \frac{a_r^3(1-\nu)}{G(t)} \Delta P(t) \left\{ 1 + \left( \frac{a_r}{H_r} \right)^3 \left( \frac{1+\nu}{10-14\nu} + \frac{15}{4} \left( \frac{H_r}{R} \right)^2 \frac{\nu-2}{5\nu-7} \right) \right\} \begin{pmatrix} x/R^3 \\ y/R^3 \\ H_r/R^3 \end{pmatrix} \quad (9)$$

where  $R = \sqrt{x^2 + y^2 + H_r^2} = \sqrt{r^2 + H_r^2}$ ,  $r$  being the horizontal distance to the pressure source.  $\nu$  is the Poisson coefficient.

### 3.2. Effective Young's Modulus and Damage Models

In the present study, we considered the volcanic edifice, loaded by the magma reservoir pressure during intereruptive periods, to be progressively and homogeneously damaged by the occurrence of ruptures (evidenced by earthquakes) weakening the edifice [see, e. g., Main, 2000; Kilburn, 2003, 2012]. We also assumed that during intereruptive inflation periods and preeruptive periods, the rupture process in the edifice is faster than healing process; therefore, edifice weakening is considered as more efficient than consolidation during these periods. Because the rupture process is continuous during these periods, damage is considered to be progressive. As a first approach, we will consider damage to remain homogeneous and isotropic throughout the intereruptive period.

Linear damage concepts have been introduced by *Kachanov* [1958] using the notion of effective stress. In this approach, the nominal or total area  $S$  on which the mean stress  $\sigma$  is applied is decomposed in a damaged area, supporting no stress, and an undamaged area  $S' = (1 - D)S$ , bearing the effective stress  $\sigma'$ . Hence,  $D$  is the proportion of damaged area. In the damage process, stress transfers to the remaining undamaged area, during small rupture events like microearthquakes. Because the force borne by the nominal surface  $S$  is actually borne by the surface  $S'$ , the effective stress is given by

$$\sigma' = \sigma \frac{S}{S'} = \frac{\sigma}{1-D} \quad (10)$$

When a uniaxial load is applied to the undamaged area, assumed to be a linear elastic body, elastic strain is given by  $\epsilon = \frac{\sigma'}{E} = \frac{\sigma}{(1-D)E}$  where  $E$  is the Young's modulus.

$$E' = (1 - D)E \quad (11)$$

is the Young's modulus of the damaged material; it is often referred to as the effective Young's modulus [see, e.g., *Kemeny and Cook*, 1986] and may be considered the large-scale Young's modulus. A similar relation also exists between the shear moduli  $G$  and  $G'$  of the undamaged and damaged material, respectively. Therefore, damage decreases the elastic coefficients of the initially perfectly elastic material. When damage increases with increasing strain,  $E'$  and  $G'$  may be represented as decreasing functions of the strain and are termed tangent moduli.

In the case of noninteracting cracks, *Walsh* [1965] showed the effective Young's modulus of an infinite 2-D elastic cracked solid to be

$$E' = \frac{E}{1 + \lambda\chi} \quad (12)$$

where  $\lambda \approx 3$  and  $\chi$  is the density of cracks in the medium. When a volume  $V$  contains  $N$  cracks  $\chi \approx \frac{Nc^3}{V}$ , where  $c^3$  is the average volume of a crack. When these cracks are distributed over an area  $S$ ,  $\chi \approx \frac{Nc^2}{S}$  where  $c^2$  is the mean surface area of a planar crack. *Budiansky and O'Connell* [1976] approximated crack interaction by assuming that each crack is surrounded by material having the effective properties of the cracked solid and found

$$E' = E(1 - \lambda\chi) \quad (13)$$

In this framework, the damage parameter  $D$  can be equated to  $\lambda\chi$ . In both *Walsh* [1965] and *Budiansky and O'Connell* [1976] approaches, cracks are assumed to preexist in the cracked elastic solid. *Bruner* [1976] modified *Budiansky and O'Connell* [1976] results by introducing cracks progressively. In this case,  $E$  varies with  $\chi$ , equation (12) may be differentiated, and the effective Young's modulus may be written

$$E' = Ee^{-\lambda\chi} \quad (14)$$

When the stressed medium is not infinite and cracks are introduced progressively, the size of the undamaged area decreases progressively and the effective stress (equation (10)) on the undamaged area progressively increases. In this case, a damage increment  $\delta$  can be defined for each rupture event, and the crack area or volume used in the previous approaches to define the crack density is replaced by the new fracture area or volume created during each rupture event. In the case of our 2-D model, the density of new fractures created can be taken to be proportional to  $\frac{\Delta c}{H}$  where  $\Delta c$  is the newly created rupture length (generally created during an earthquake) and  $H$  is the length to be ruptured during the complete rupture (diking) process, assuming that both the new fracture area and the area to be ruptured have the same out-of-plane unit length. In our model, in which we assume that healing processes are slower than damage processes,  $H$  can be considered to be the depth of the roof of the magma reservoir, which is a minimum estimate for  $H$ . At each step  $i$ ,

$$\sigma'_{i+1} = \frac{\sigma'_i}{1 - \delta} \quad (15)$$

which leads to

$$E'_{i+1} = E'_i(1 - \delta) \quad (16)$$

where  $\delta = \frac{\Delta c}{H}$ . After  $N$  rupture events, the effective Young's modulus  $E'_N$  is merely

$$E'_N = E_0(1 - \delta)^N \quad (17)$$

This conclusion was already reached by *Amitrano and Helmstetter* [2006]. In this case, the total damage  $D$  due to the occurrence of  $N$  consecutive rupture events, each producing the damage increment  $\delta$  is

$$D = 1 - (1 - \delta)^N \quad (18)$$

Hence, this is a power-law, progressive damage model. Linearizing equation (17) would give

$$E'_N = E_0(1 - N\delta) \quad (19)$$

This corresponds to the creation of a new fracture length  $N\Delta c$  under the initial stress conditions. This approximation is valid only when there are no or very few crack interactions, that is, when the newly created fracture length remains diffuse and small relative to the length remaining to be ruptured.

When rupture events are earthquakes recorded by a seismic network on a volcano, the rate of which being counted daily, the effective Young's modulus can be written

$$E'_N = E_0 \prod_{i=1}^{i=N} (1 - \delta_i)^{\delta_i} \quad (20)$$

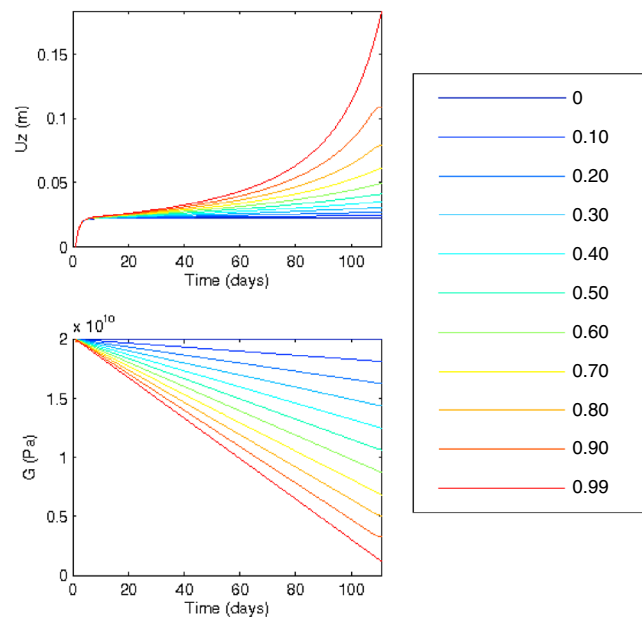


**Figure 5.** Theoretical vertical surface displacement  $u_z$  (computed for a horizontal offset  $r = 0$  (Figure 4) from equations (8) and (9)) and shear modulus  $G$  as a function of time for a wide interval of total damage  $D$  (color), damage rate being constant.

where  $N$  is the number of days in the earthquake rate daily time series,  $n_i$  is the number of earthquakes occurring during day  $i$  (the daily seismicity rate), and  $\delta_i$  is the damage increment occurring during each day  $i$ . In this case, the effective Young's modulus decreases with seismicity rate, as found in rock fracture experiments [see, e.g., Heap *et al.*, 2009, 2010].  $\delta_i$  may vary with time, taking into account the changes in magnitude and characteristic size of the earthquakes recorded during day  $i$ .

### 3.3. Effects of Source, Material and Damage Parameters on Surface Deformation

The model described by equations (8) and (9) has seven parameters characterizing the geometry, material properties (initial rock shear modulus and magma viscosity), pressure conditions at the bottom of the pipe, and one incremental damage parameter  $\delta_i$  per time step. We termed

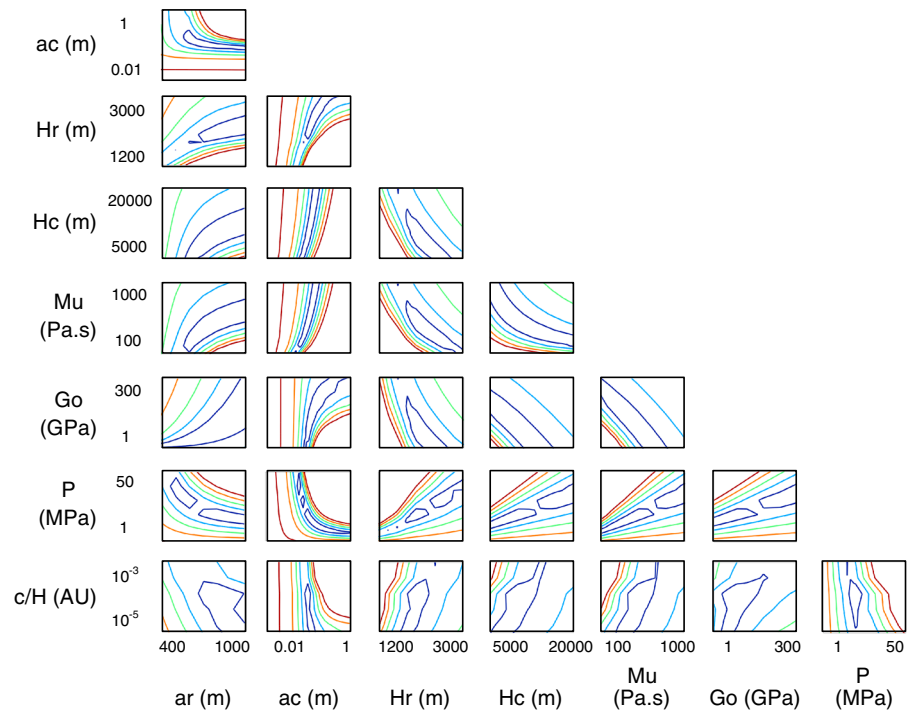
the geometrical and pressure parameters, source parameters. Source and material parameters control the part of the surface displacement signal that occurs when there is no or a few seismicity and therefore no damage, generally at the beginning of an interruptive period, when the reservoir pressure begins to increase. Surface displacements measured during such periods are mostly low-frequency signals. The incremental damage parameter controls the part of the surface displacement signal that occurs when seismicity increases, generally during the preeruptive period. Therefore, source and material parameters, on the one hand, and the incremental damage parameter, on the other hand, are weakly coupled.

Figure 5 shows the effect of damage on the surface displacement, when a simple linear damage model was used with a constant damage time rate. It shows that damage may explain the acceleration in surface displacement, if the constant damage rate is sufficient. Surface displacement bifurcates from the stable elastic solution when damage is null to instability when damage reaches a sufficient level. In our model, the incremental damage is the ratio of the incremental rupture length to the length to be ruptured (typically the depth of the magma reservoir roof); therefore, it shows that superficial magma reservoirs are potentially more instable than deeper reservoirs for a given set of pressure conditions, material parameters, incremental rupture length, and magma feeding system geometry.

## 4. Inversion

In order to investigate more thoroughly whether or not damage processes efficiently explain accelerations in surface displacements, we had to estimate the order of magnitude of the incremental damage parameter from surface displacement data and then compare this parameter with physically admissible values for this parameter. To this end, we performed an inversion of the surface displacement data in order to estimate the model parameters. Because the coupling between source/material parameters and incremental damage parameter is weak, it is possible to perform the inversion by independently estimating the source and material parameters (determined for a given incremental damage parameter) and then the incremental damage parameter itself.

Therefore, the first stage of the inversion involved estimating seven parameters:  $a_r, a_c, H_r, H_c, \mu, G_0, P$ . Due to the number of these parameters and the nonlinearity of the relations between them, we first explored the parameter space in order to represent the relations between the parameters (trade-offs), which control



**Figure 6.** Vertical displacement misfit function as a function of all possible model parameter pairs. In each plot, the corresponding parameter pair varies within a given range, whereas other parameters are kept constant:  $a_r = 800$  m,  $a_c = 0.5$  m,  $H_r = 2000$  m,  $H_c = 10000$  m,  $\mu = 100$  Pa.s,  $G_0 = 30$  GPa,  $P = 20$  MPa,  $\delta = \frac{c}{H} = 5.10^{-4}$ . Misfit function contour level increases from 3 cm (dark blue) to 15 cm (dark red), with a 3 cm step.

the probability density function and the uncertainty on the parameters. We estimated these trade-offs by systematically computing the misfit function  $(u_{th} - d)^T C_d^{-1} (u_{th} - d)$  (where  $u_{th}$  is the modeled displacement,  $d$  is the observed displacement (data), both being functions of time, and  $C_d$  is the data covariance matrix) in the parameter space. We then represented this misfit function in two-dimensional subspaces of parameters (Figure 6). Intervals of the parameter space that were systematically and uniformly explored were determined using previous geological and geophysical studies on Piton de la Fournaise [Peltier et al., 2007; Prôno et al., 2009].

Results (Figure 6) showed a wide range of source and material parameter values that fit the surface displacement data equally well. Therefore, trade-offs between model parameters may be quite marked due to (1) the simple form of the time evolution of the overpressure when damage is weak (see, e.g., equation (6)), which is mostly controlled by one almost constant parameter, the pseudo-characteristic time  $\tau^*$ , and (2) the fact that  $\tau^*$  depends on five physical parameters. The relation between these five parameters reveals most of the trade-offs between the source/material parameters.

Due to the nonlinearity of the relation between the data and model parameters, we performed the inversion using a genetic algorithm with a roulette selection. Figure 7 shows the results of 10 inversions that fit the data with the same residual standard deviation. It shows that although the values obtained for source and material parameters may differ substantially, their coherent variation mostly controls the amplitude of the results (time variation in the shear modulus, reservoir overpressure, volume variation, magma flow) but does not greatly affect the shape of their time variations. Hence, it is not necessary to know the exact characteristics of the source and material model in order to explain interruptive accelerations: these accelerations are similar for a large number of coherent source and material parameter combinations, and they are mostly controlled by damage.

Consequently, in the inversion for the incremental damage parameter  $\delta_i$ , source and material parameters were fixed at values that best fit the displacement data, especially at the beginning of the interruptive period, when damage is weak. We used (Figure 6)  $a_c = 800$  m,  $a_r = 0.5$  m,  $H_r = 2000$  m,  $H_c = 10000$  m,

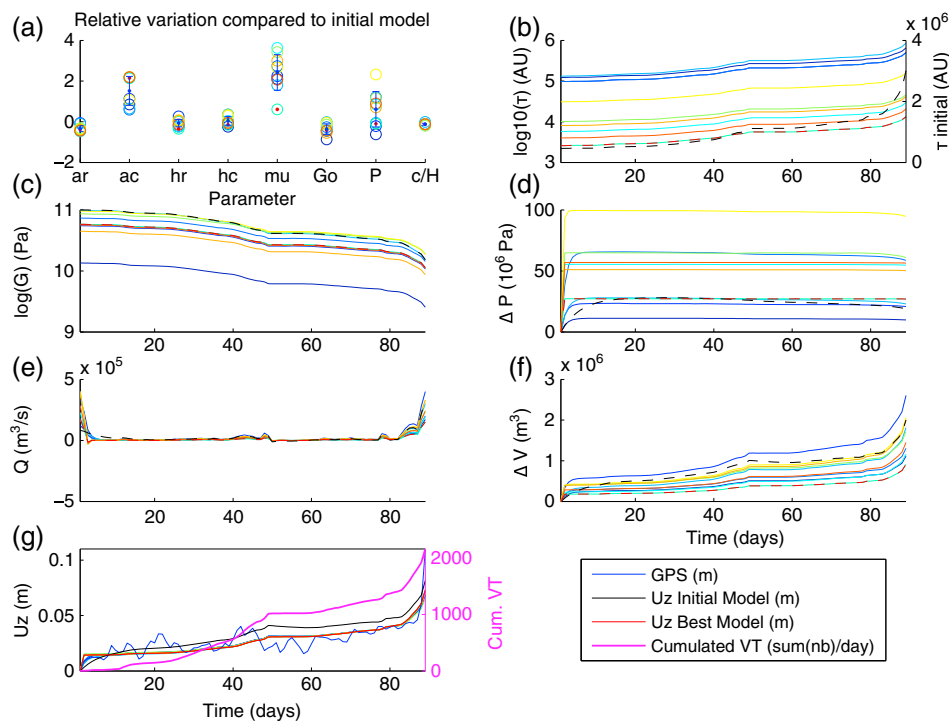


**Figure 7.** Results of 10 inversions of source and material model parameters using a constant incremental damage parameter for station DERG (see Figure 1 for its location). (a) Relative variation of each parameter (see text for the reference values used in the initial model), (b) pseudo-characteristic time, (c) logarithm of shear modulus, (d) over-pressure in the reservoir, (e) magma flow rate, (f) variation in reservoir volume, and (g) observed (blue) and modeled (red) vertical displacement compared to initial model (black). Colors for  $G$ ,  $\Delta P$ ,  $Q$  and  $\Delta V$  correspond to those used in Figure 7a; dashed lines correspond to the initial (black) and best (red) model. In Figure 7g, all modeled vertical displacements are superposed onto the best (red) model. The last day shown corresponds to the beginning of the 30 March to 1 May 2007 eruption.

$\mu = 100 \text{ Pa s}$ ,  $G_0 = 30 \text{ GPa}$ ,  $P = 20 \text{ MPa}$ . We obtained the final fit of the preeruptive displacement accelerations by inverting the incremental damage parameter  $\delta_i$  as a function of time, using the same genetic algorithm used for the source and material parameters, and exploring the interval  $[5 \cdot 10^{-5}, 5 \cdot 10^{-3}]$ .

### 5. Results and Discussion

In this initial study, we focused on the preeruptive dynamics and time evolution of the model parameters, rather than on the spatial distribution of damage or on strain localization. Figures 8–10 show that vertical displacement, incremental damage, shear modulus  $G$ , and overpressure  $\Delta P$  depend on the GPS station location (Figure 1). A complete interpretation would require using a tensorial approach in order to take into account damage anisotropy. However, although the progressive localization of the strain along the plane of a future dike involves an anisotropic damage process, displacements measured on Piton de la Fournaise exhibit a strong East/West asymmetry (Figure 1; see also, e.g., Got *et al.* [2013]) that tends to hide the anisotropic component of the deformation. Consequently, in the present study, we restricted our analysis to vertical displacements, using a simple scalar approach and making no attempt to spatialize damage.

Our results (Figures 8–10) show that incremental damage is roughly constant and scales the decrease of the shear modulus  $G$ , which remains roughly proportional to the seismicity rate. Minimum  $G$  is an order of magnitude lower and maximum overpressure  $\Delta P$  is 1.3 to 5 times lower than the values found for the reference elastic solution. Volume increases by 2 to 5 relative to the elastic solution. Finally, vertical displacement accelerates, as the decrease in  $G$  is greater than the decrease in  $\Delta P$ .  $\Delta P$  was taken to be zero on 1 January 2007, so our computations indicate the change in overpressure since that date.  $\Delta P$  was similar for the elastic and damaged cases when the cumulated number of earthquake was low (during the first

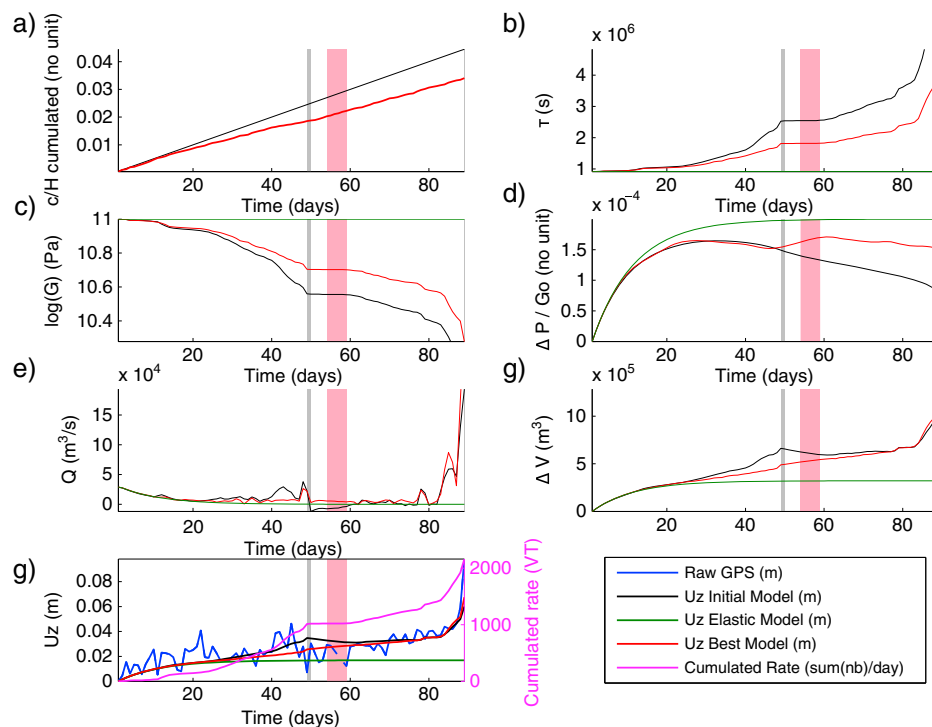


**Figure 8.** Model variables as a function of time, from 1 January 2007 to 30 March 2007, after inversion at the SNEG station (Figure 1). (a) Cumulated normalized rupture length, (b) pseudo-characteristic time, (c) logarithm of shear modulus, (d) adimensional over-pressure in the reservoir, (e) magma flow rate, (f) reservoir volume change, and (g) measured (blue) and modeled (red) vertical displacement compared to the initial model (black), and seismicity rate (purple). Black and red solid lines show the initial and the best model resulting from inversion, respectively. Vertically shaded grey and pink areas indicate the periods of the 18–19 February 2007 eruption and Gamède storm, respectively. The last day shown corresponds to the beginning of the 30 March to 1 May 2007 eruption.

10 days). Subsequently, overpressure increased up to day 20 (20 January 2007), after which it remained more or less constant for almost 30 days (with a short period when it decreased before the 18 February eruption). Day 20 was the day on which yield strength was reached, and the earthquake rate began to accelerate in a single phase that continued to day 48 (eruption of 18 February 2007). Overpressure increased immediately after the 18 February eruption, reaching a maximum at around day 60, when the earthquake rate and vertical displacement increased and accelerated again (up to the beginning of the 30 March to 1 May eruption). There was a general decrease in overpressure at day 80, about 10 days before the 30 March eruption. Final overpressure was about 50% lower than the reference elastic overpressure.

By inverting the incremental damage parameter, we were able to compare its values with rupture length estimates obtained from seismicity analysis. Results (Figures 8–10) of the inversion for the incremental damage parameter  $\delta = \frac{\Delta c}{H}$  show that it can take values within a very limited interval, so its value during the intereruptive period may be considered as sufficiently constant for it to be used as a unique parameter for each station. Therefore, total damage is a quasi-linear function of seismicity rate. Thus, this simple model of homogeneous isotropic damage reproduces the first-order trends of a relatively complex intereruptive dynamics during tens of days, with the addition of just one new parameter compared with the reference elastic model. It accounts for the vertical displacement observed, with a constant incremental damage parameter  $\delta$  comprised between  $1 \cdot 10^{-4}$  and  $1 \cdot 10^{-3}$  per day in a vertical diametral plane of the Dolomieu crater. Given that the reservoir roof is  $H \sim 2.5$  km below the summit, it means that the incremental rupture length is of the order of  $\sim 1$  m per day and per unit length in the horizontal out-of-plane direction.

These values have to be compared with the quasi-constant earthquake rupture length (Figure 3) inferred from Wells and Coppersmith [1994]’s magnitude–rupture length relationships. Cumulated rupture length computed for the  $\sim 55000$  earthquakes with a characteristic rupture length of  $\sim 66$  m per earthquake (consistent with results from earthquake spectra published by De Barros et al. [2013]) is  $\sim 3600$  km in

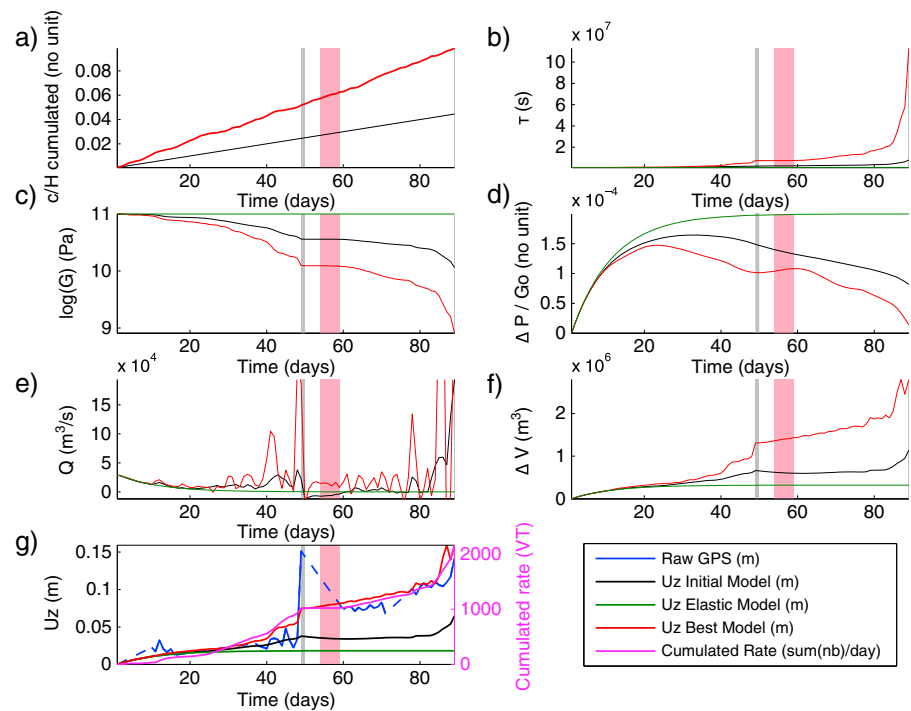


**Figure 9.** Model variables as a function of time, from 1 January 2007 to 30 March 2007, after inversion at the DSRG station (Figure 1). (a) Cumulated normalized rupture length, (b) pseudo-characteristic time, (c) logarithm of shear modulus, (d) adimensional over-pressure in the reservoir, (e) magma flow rate, (f) reservoir volume change, and (g) measured (blue) and modeled (red) vertical displacement compared to the initial model (black), and seismicity rate (purple). Black and red solid lines show the initial and the best model resulting from inversion, respectively. Vertically shaded grey and pink areas indicate the periods of the 18–19 February 2007 eruption and Gamède storm, respectively. The last day shown corresponds to the beginning of the 30 March to 1 May 2007 eruption.

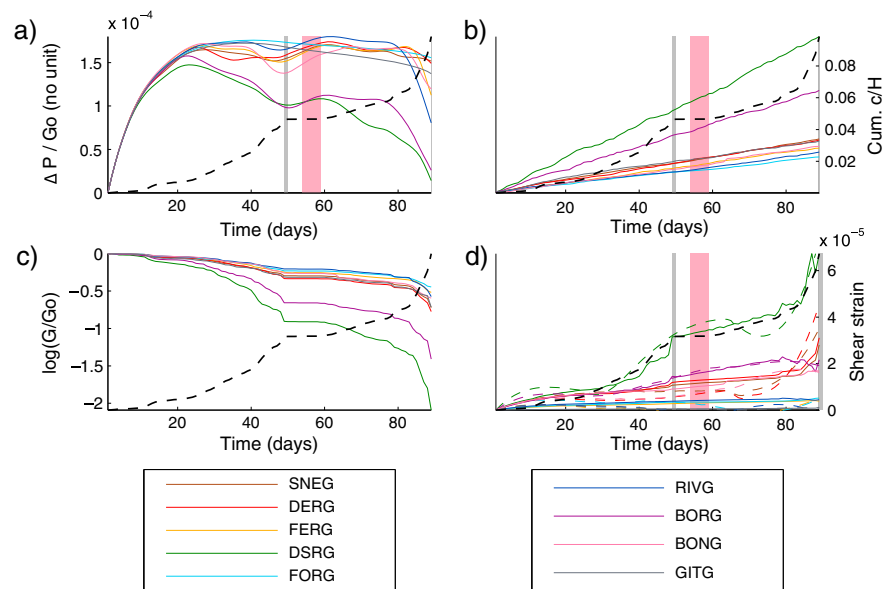


**Figure 10.** Model variables as a function of time for all OVPF geodetic stations (in color) from 1 January 2007 to 30 March 2007, after inversion. (a) Adimensional overpressure in the reservoir, (b) cumulated normalized rupture length, (c) logarithm of adimensional shear modulus, and (d) shear strain: computed from modeled displacements (colored solid line) and from data (colored dashed line). Black dashed line shows the cumulative seismicity rate. Vertically shaded grey and pink areas indicate periods of the 18–19 February 2007 eruption and Gamède storm, respectively. The last day shown corresponds to the beginning of the 30 March to 1 May 2007 eruption.

10 years, that is,  $\sim 1$  km per day, in the  $\sim 2.5$  km<sup>3</sup> volume of the Dolomieu crater between the surface and the reservoir roof. The characteristic horizontal dimension of Dolomieu crater is its  $\sim 1$  km diameter. Therefore, the mean daily rupture length inferred from earthquake magnitudes in a vertical plane is  $\sim 1$  m per day and per unit length in the horizontal out-of-plane direction, which is the order of magnitude as that inferred using our damage approach. Constant rupture length, with similar and realistic orders of magnitude inferred from both earthquake magnitude and damage, contributes to validate the progressive power-law damage model used in this study. It also shows that during intereruptive and preeruptive periods, damage and stress transfer mainly occur through an increase in the number of rupture events and not by an increase in earthquake rupture area or magnitude. Another conclusion that may be reached from this brief analysis of the intensity of the seismic fracturation process on Piton de la Fournaise is that healing processes are likely to be continuously at work to account for the long-term strength of the volcanic edifice. Preeruptive periods are periods where damage processes are stronger than healing processes. Analyses of seismic noise correlation or shear-wave splitting by *Clarke et al.* [2013], *Rivet et al.* [2014], and M. Savage et al. (Seismic anisotropy and its precursory change before eruptions at Piton de la Fournaise volcano, La Réunion, submitted to *Journal of Geophysical Research*, 2015) revealed decreases in seismic velocities during preeruptive periods at Piton de la Fournaise, which may be related to progressive damage processes.

During intereruptive and preeruptive periods, earthquake interaction, damage, and stress transfer dynamics remain moderate. The acceleration in seismicity rate shows that stress transfer is probably greater at the end of the preeruptive period, which can therefore be considered as the preparation of an instability that will lead to a rupture process. It is likely that increased rupture areas and large-scale ruptures appear at the beginning of the eruptive process, when seismic records show that earthquake waveforms overlap, large seismic energy releases, and eruptive tremor occurs. Careful study of the microseismicity preceding the 14–31 October 2010 eruption at Piton de la Fournaise showed that earthquake ruptures have occurred at the surface close to the eruption site three hours before the eruption [*De Barros et al.*, 2013]. *Bean et al.* [2014] studied long-period seismicity at the Etna (Italy), Turrialba (Costa Rica), and Ubinas (Peru) volcanoes. They showed that short-duration, long-period events cannot be generated by resonance in fluid-filled cavities and are best explained by slow-rupture failure of shallow unconsolidated volcanic materials. Hence, damage can widely facilitate magma propagation in the edifice, at low pressure, by preparing its path up to the surface by a fracture process zone, a classical concept in fracture mechanics [see, e.g., *Dugdale*, 1960; *Barenblatt*, 1962; *Zang et al.*, 2000; *de Borst*, 2002]. It is currently thought that preeruptive tremor arises from high velocity propagation of pressurized magma in dikes or conduits. According to Poiseuille's law, magma flow is proportional to the pressure gradient along the dike or conduit; therefore, high velocity propagation implies that pressure gradient is high. As pressure variations in the magma reservoir are not large and rapid, high-velocity magma propagation to the surface implies that pressure and strength along the future dike path or conduit are low. Rock ruptures and creates volume before magma propagation, far ahead of the magma front.

Figures 8–10 show that magma reservoir overpressure generally decreased before the two eruptions (18–19 February and 30 March to 1 May) that occurred during this period. This decrease in pressure was due to the nonlinear increase in reservoir volume, which was due to the decrease in  $G$  consecutive to the increase in damage. Finally, surface deformation increased when overpressure decreased because  $G$  decreased faster than the overpressure. No or a few seismicity occurred after the eruption,  $G$  remained stable, and the pressure gradient in the deep magma conduit allowed the reservoir pressure to grow. Other nonlinear processes may occur, mostly at the end of the preeruptive period, as damage and strain localize and produce anisotropic surface deformation, strain weakening, an increase in permeability, fluid migration, gas exsolution, and pressurization in anisotropic structures like dikes. These processes may amplify the nonlinear acceleration at the end of the preeruptive period, and they are not taken into account by our simple model. However, our results illustrate the importance of including a realistic, nonlinear rheology for the volcanic edifice when modeling edifice reaction, magma-edifice interactions, and magma migration into the edifice. This is especially true for inferring realistic magma pressures and eruptive dynamics, and for modelling gas exsolution and/or magma pumping during the last preeruptive stages: magma can decompress without ascension when rock yield strength is reached. *Currenti et al.* [2010] and *Gregg et al.* [2012] showed that the use of elastoplastic or thermomechanic modeling leads to lower pressures in the magma reservoirs than previously thought by using elastic modeling. Pressure decreases and complex

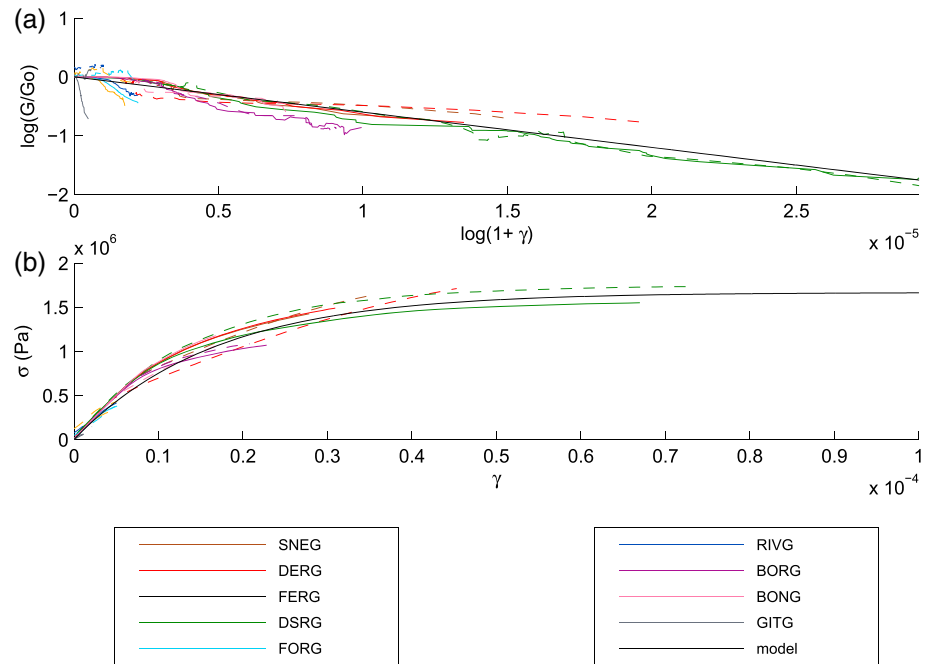


**Figure 11.** (a) Logarithm of the adimensional shear modulus and (b) shear strength (in Pa) as a function of shear strain  $\gamma$  (computed from modeled displacements: solid line; from data: dashed line) for all OVPF geodetic stations (in color) from 1 January 2007 to 30 March 2007. Black solid lines in Figures 11a and 11b represent the model described, respectively, by equations (21) and (22).

nonlinear behaviors when damage increases are also evidenced during fluid injection and hydraulic fracturing (see, e.g., *Shalev and Lyakhovskiy* [2013]).

Pressure decreases in magma reservoirs may also be at the origin of pauses or episodic behaviors (episodes of quietness during a long-term eruptive process; see, e.g., *Boichu et al.* [2008]) or even the chaotic behaviors that sometimes occur during large eruptions of basaltic or andesitic volcanoes [see, e.g., *Budi-Santoso et al.*, 2013]. Such chaotic behaviors increase the unpredictability of the evolution of the system and increase the modeling error variance of the constant-load prediction approaches like FFM (see, e.g., A. Boué et al., submitted manuscript, 2015). It therefore decreases the accuracy of their eruption predictions, which may limit their application. More generally, the edifice processes at work during the preeruptive and eruptive stages may greatly contribute to the eruptive process: damage reduces the strength of the edifice and it increases its permeability to gas [see, e.g., *Gueguen and Schubnel*, 2003; *Nara et al.*, 2011]. The associated deformation results in a nonlinear increase in the reservoir volume and a decrease in its pressure and may induce gas exsolution, magma recharge, and further interactions with the mantle. Healing and consolidation occur during the whole process. Hence, a volcano's eruptive history results from the competition of all these edifice and magmatic processes. In order to determine this history, it is necessary to firmly establish the relations between geophysical observables (deformation, seismicity, gas flux) and the model parameters.

Figure 11 shows  $G$  and edifice strength as a function of shear strain  $\gamma$ . We computed shear strain by defining a radial vector linking the center of the magma reservoir to the geodetic station and an orthoradial vector linking the station to our geometrical model's vertical axis of symmetry (Figure 4). We calculated shear strain in the radial direction as the ratio of the displacement projected on the orthoradial vector, to the length of the radial vector.  $G$  was found to fit to a simple function of  $\gamma$ :

$$G = G_0(1 + \gamma)^\alpha \tag{21}$$

with  $\alpha \approx -6.10^4$ . Integrating  $G$  over shear strain gave an estimation of the pre-peak shear strength (reaction) of the rocks on the volcanic edifice scale (Figure 11):

$$\sigma(\gamma) = \frac{G_0}{\alpha + 1} \left( (1 + \gamma)^{(\alpha+1)} - 1 \right) \tag{22}$$

It shows that shear strength tends to a relatively limited value for large shear strains, which means the edifice actually tends to plasticity above a certain strain. This result helps quantify the partitioning of elastic and plastic strain in the edifice. It shows that at most stations, about 50% of the total strain during interruptive and preeruptive periods is purely elastic strain, whereas for large strains, this ratio drops to less than 20%. Thus, plastic deformation is an important feature of the Piton de la Fournaise volcanic edifice, a conclusion which confirms former results [Got *et al.*, 2013]. Such studies can be performed on other well-instrumented large basaltic shield volcanoes. The present study, focused on the prepeak behavior of the Piton de la Fournaise volcanic edifice, completes [Got *et al.*, 2013]'s study focused on its postpeak behavior.

## 6. Conclusion

In this work we have used numerical modeling and inversion to study surface displacements of a volcanic edifice submitted to the pressure of a magma reservoir, paying special attention to cases where seismicity and surface displacements accelerate at the end of interruptive periods. We showed that the acceleration in surface deformation can be explained by a model of pressurized reservoir embedded in an elastic medium with constant pressure at the base of the feeding system, progressively damaged by rupture events at a rate given by the observed seismicity rate. Progressive damage is modelled by the progressive weakening of the elastic moduli, using a power-law damage model in order to take into account crack interaction in the reservoir roof. We found that during the interruptive and preeruptive periods, incremental damage is constant and shear modulus is inversely proportional to shear strain, so shear strength reaches a limiting value at which strain is plastic. This model is able to explain stable states and moderate or accelerating surface displacement rates, depending on the value assigned to the damage parameter. Consequently, the model is capable of reproducing the bifurcation between stable and unstable states, and the large range of dynamics observed during the interruptive periods. Damage weakens the edifice, which induces the increase in reservoir volume and the decrease in reservoir pressure. This pressure decrease may induce other nonlinear processes: gas exsolution, or magma recharge from mantle source, which lead to instability. The interplay between reservoir pressure increase, subsequent nonlinear weakening of the edifice, increase in permeability, subsequent pressure decrease, and healing/consolidation of the edifice may be responsible for the episodic or chaotic behavior of the eruptive history of active volcanoes over various time scales.

## Acknowledgments

Authors acknowledge the "Géophysique des Volcans" CNRS team and the ISTerre laboratory for funding this study. The data used in this paper were collected by the Observatoire Volcanologique du Piton de la Fournaise / Institut de Physique du Globe de Paris (OVPF/IPGP). They acknowledge Svetlana Byrdina, Marie Boichu, David Marsan, Michael Heap, and Nicolas Fournier for their careful reviews, Svetlana Byrdina for her help in graphics, and Paul Henderson for the English rewording.

## References

- Agnon, A., and V. Lyakhovskiy (1995), Damage distribution and localization during dyke intrusion, in *The Physics and Chemistry of Dykes*, edited by G. Baer and A. Heimann, pp. 65–78, Balkema, Rotterdam, Netherlands.
- Amitrano, D., and A. Helmstetter (2006), Brittle creep, damage, and time to failure in rocks, *J. Geophys. Res.*, *111*, B11201, doi:10.1029/2005JB004252.
- Bachèlery, P. (1981), Le Piton de La Fournaise (île de la Réunion), Etude volcanologique structurale, Thèse, Université de Clermont-Ferrand, France.
- Barenblatt, G. (1962), The mathematical theory of equilibrium cracks in brittle fracture, *Adv. Appl. Mech.*, *7*, 55–129.
- Bean, C., L. De Barros, I. Lokmer, J.-P. Métaxian, G. O'Brien, and S. Murphy (2014), Long-period seismicity in the shallow volcanic edifice formed from slow-rupture earthquakes, *Nat. Geosci.*, *7*, 71–75.
- Bell, A., J. Greenhough, M. Heap, and I. Main (2011a), Challenges for forecasting based on accelerating rates of earthquakes at volcanoes and laboratory analogues, *Geophys. J. Int.*, *185*, 718–723.
- Bell, A., M. Naylor, M. Heap, and I. Main (2011b), Forecasting volcanic eruptions and other material failure phenomena: An evaluation of the failure forecast method, *Geophys. Res. Lett.*, *38*, L15304, doi:10.1029/2011GL048155.
- Benson, P., B. Thompson, P. Meredith, S. Vinciguerra, and R. Young (2007), Imaging slow failure in triaxially deformed Etna basalt using 3D acoustic-emission location and X-ray computed tomography, *Geophys. Res. Lett.*, *34*, L03303, doi:10.1029/2006GL028721.
- Blake, S. (1984), Volatile oversaturation during the evolution of silicic magma chambers as an eruption trigger, *J. Geophys. Res.*, *89*, 8237–8244.
- Boichu, M., B. Villemant, and G. Boudon (2008), A model for episodic degassing of an andesitic magma intrusion, *J. Geophys. Res.*, *113*, B07202, doi:10.1029/2007JB005130.
- Bonforte, A., A. Bonaccorso, F. Guglielmino, M. Palano, and G. Puglisi (2008), Feeding system and magma storage beneath Mt. Etna as revealed by recent inflation/deflation cycles, *J. Geophys. Res.*, *113*, B05406, doi:10.1029/2007JB005334.
- Bruner, W. (1976), Comment on "Seismic velocities in dry and saturated cracked solids" by O'Connell and Budiansky, *J. Geophys. Res.*, *81*, 2573–2576.
- Budiansky, B., and R. O'Connell (1976), Elastic moduli of a cracked solid, *Int. J. Solids Struct.*, *12*, 81–97.
- Budi-Santoso, A., P. Lesage, S. Dwiyo, S. Sumarti, Subandriyo, Surono, P. Jousset, and J.-P. Metaxian (2013), Analysis of the seismic activity associated with the 2010 eruption of Merapi Volcano, Java, *J. Volcanol. Geotherm. Res.*, *261*, 153–170.
- Clarke, D., F. Brenguier, J.-L. Froger, N. Shapiro, A. Peltier, and T. Staudacher (2013), Timing of a large volcanic flank movement at Piton de la Fournaise volcano using noise-based seismic monitoring and ground deformation measurements, *Geophys. J. Int.*, *195*(2), 1132–1140.

- Cox, S., and P. Meredith (1993), Microcrack formation and material softening in rock measured by monitoring acoustic emissions, *Int. J. Rock Mech. Min. Sci. Geomech. Abstr.*, *30*, 11–24.
- Currenti, G., A. Bonaccorso, C. Del Negro, D. Scandura, and E. Boschi (2010), Elasto-plastic modeling of volcano ground deformation, *Earth Planet. Sci. Lett.*, *296*, 311–318.
- De Barros, L., C. Bean, M. Zecevic, F. Brenguier, and A. Peltier (2013), Eruptive fracture location forecasts from high-frequency events on Piton de la Fournaise Volcano, *Geophys. Res. Lett.*, *40*, 4599–4603, doi:10.1002/grl.50890.
- de Borst, R. (2002), Fracture in quasi-brittle materials: A review of continuum damage-based approaches, *Eng. Fract. Mech.*, *69*, 95–112.
- Delaney, P., and D. McTigue (1994), Volume of magma accumulation or withdrawal estimated from surface uplift or subsidence, with application to the 1960 collapse of Kilauea Volcano, *Bull. Volcanol.*, *56*(6–7), 417–424.
- Dugdale, D. (1960), Yielding of steel sheets containing slits, *J. Mech. Phys. Solids*, *8*, 100–104.
- Gerbault, M., F. Cappa, and R. Hassani (2012), Elasto-plastic and hydromechanical models of failure around an infinitely long magma chamber, *Geochem. Geophys. Geosyst.*, *13*, Q03009, doi:10.1029/2011GC003917.
- Got, J.-L., A. Peltier, T. Staudacher, P. Kowalski, and P. Boissier (2013), Edifice strength and magma transfer modulation at Piton de la Fournaise volcano, *J. Geophys. Res. Solid Earth*, *118*, 5040–5057, doi:10.1002/jgrb.50350.
- Gregg, P., S. de Silva, E. Grosfils, and J. Parmigiani (2012), Catastrophic caldera-forming eruptions: Thermomechanics and implications for eruption triggering and maximum caldera dimensions on Earth, *J. Volcanol. Geotherm. Res.*, *241–242*, 1–12.
- Gudmundsson, A. (2006), How local stresses control magma-chamber ruptures, dyke injections, and eruptions in composite volcanoes, *Earth Sci. Rev.*, *79*, 1–31.
- Gueguen, Y., and A. Schubnel (2003), Elastic wave velocities and permeability of cracked rocks, *Tectonophysics*, *370*, 163–176.
- Heap, M., S. Vinciguerra, and P. Meredith (2009), The evolution of elastic moduli with increasing crack damage during cyclic stressing of a basalt from Mt. Etna volcano, *Tectonophysics*, *471*, 153–160.
- Heap, M., D. Faulkner, P. Meredith, and S. Vinciguerra (2010), Elastic moduli evolution and accompanying stress changes with increasing crack damage: Implications for stress changes around fault zones and volcanoes during deformation, *Geophys. J. Int.*, *183*, 225–236.
- Heap, M., P. Baud, P. Meredith, S. Vinciguerra, A. Bell, and I. Main (2011), Brittle creep in basalt and its application to time-dependent volcano deformation, *Earth Planet. Sci. Lett.*, *307*, 71–82.
- Kachanov, L. (1958), Time of the rupture process under creep conditions, *Isv. Akad. Nauk. SSR. Otd. Tekh. Nauk*, *8*, 26–31.
- Kemeny, J., and N. Cook (1986), Effective moduli, non-linear deformation and strength of a cracked elastic solid, *Int. J. Rock Mech. Min. Sci. Geomech. Abstr.*, *23*, 107–118.
- Kilburn, C. (2003), Multiscale fracturing as a key to forecasting volcanic eruptions, *J. Volcanol. Geotherm. Res.*, *125*, 271–289.
- Kilburn, C. (2012), Precursory deformation and fracture before brittle rock failure and potential application to volcanic unrest, *J. Geophys. Res.*, *117*, B02211, doi:10.1029/2011JB008703.
- Lengliné, O., D. Marsan, J. Got, V. Pinel, V. Ferrazzini, and P. Okubo (2008), Seismicity and deformation induced by magma accumulation at three basaltic volcanoes, *J. Geophys. Res.*, *113*, B12305, doi:10.1029/2011JB008703.
- Letourneur, L., A. Peltier, T. Staudacher, and A. Gudmundsson (2008), The effects of rock heterogeneities on dyke paths and asymmetric ground deformation: The example of Piton de la Fournaise volcano (La Réunion Island), *J. Volcanol. Geotherm. Res.*, *173*(3–4), 289–302.
- Lisowski, M. (2007), Analytical volcano deformation source models, in *Volcano Deformation*, edited by D. Dzurisin, pp. 279–304, Springer, Heidelberg, Berlin.
- Main, I. (2000), A damage mechanics model for power-law creep and earthquake aftershock and foreshock sequences, *Geophys. J. Int.*, *142*, 151–161.
- Massin, F., V. Ferrazzini, P. Bachèlery, A. Nercessian, Z. Duputel, and T. Staudacher (2011), Structures and evolution of the plumbing system of Piton de la Fournaise volcano inferred from clustering of 2007 eruptive cycle seismicity, *J. Volcanol. Geotherm. Res.*, *202*, 96–106.
- McLeod, P., and S. Tait (1999), The growth of dykes from magma chambers, *J. Volcanol. Geotherm. Res.*, *92*, 231–246.
- Mériaux, C., J. Lister, V. Lyakhovskiy, and A. Agnon (1999), Dyke propagation with distributed damage of the host rock, *Earth Planet. Sci. Lett.*, *165*, 177–185.
- Michon, L., F. Saint-Ange, P. Bachèlery, N. Villeneuve, and T. Staudacher (2007), Role of the structural inheritance of the oceanic lithosphere in the magmato-tectonic evolution of Piton de La Fournaise volcano (La Réunion Island), *J. Geophys. Res.*, *112*, B04205, doi:10.1029/2006JB004598.
- Montgomery-Brown, E., D. Sinnett, K. Larson, M. Poland, P. Segall, and A. Miklius (2011), Spatiotemporal evolution of dike opening and décollement slip at Kilauea volcano, Hawai'i, *J. Geophys. Res.*, *116*, B03401, doi:10.1029/2010JB007762.
- Nara, Y., P. Meredith, T. Yoneda, and K. Kaneko (2011), Influence of macro-fractures and micro-fractures on permeability and elastic wave velocities in basalt at elevated pressure, *Tectonophysics*, *503*, 52–59.
- Nercessian, A., A. Hirn, J.-C. Lépine, and M. Sapin (1996), Internal structure of Piton de la Fournaise volcano from seismic wave propagation and earthquake distribution, *J. Volcanol. Geotherm. Res.*, *70*, 123–143.
- Peltier, A., V. Ferrazzini, T. Staudacher, and P. Bachèlery (2005), Imaging the dynamics of dyke propagation prior to the 2000–2003 flank eruptions at Piton de la Fournaise, Réunion Island, *Geophys. Res. Lett.*, *32*, L22302, doi:10.1029/2005GL023720.
- Peltier, A., T. Staudacher, P. Catherine, L.-P. Ricard, P. Kowalski, and P. Bachèlery (2006), Subtle precursors of volcanic eruptions at Piton de la Fournaise detected by extensometers, *Geophys. Res. Lett.*, *33*, L06315, doi:10.1029/2005GL025495.
- Peltier, A., T. Staudacher, and P. Bachèlery (2007), Constraints on magma transfers and structures involved in the 2003 activity at Piton de la Fournaise from displacement data, *J. Geophys. Res.*, *112*, B03207, doi:10.1029/2006JB004379.
- Peltier, A., V. Famin, P. Bachèlery, V. Cayol, Y. Fukushima, and T. Staudacher (2008), Cyclic magma storages and transfers at Piton de la Fournaise volcano (La Réunion hotspot) inferred from deformation and geochemical data, *Earth Planet. Sci. Lett.*, *270*(3–4), 180–188.
- Peltier, A., P. Bachèlery, and T. Staudacher (2009a), Magma transfer and storage at Piton de la Fournaise (La Réunion) between 1972 and 2007: A review of geophysical and geochemical data, *J. Volcanol. Geotherm. Res.*, *184*(1–2), 93–108.
- Peltier, A., T. Staudacher, P. Bachèlery, and V. Cayol (2009b), Formation of the April 2007 caldera collapse at Piton de la Fournaise volcano: Insights from GPS data, *J. Volcanol. Geotherm. Res.*, *184*(1–2), 152–163.
- Pinel, V., and C. Jaupart (2003), Magma chamber behaviour beneath a volcanic edifice, *J. Geophys. Res.*, *108*(B2), 2072, doi:10.1029/2002JB001751.
- Press, W. H. (1992), *Numerical Recipes in Fortran 77: The Art of Scientific Computing*, vol. 1, Cambridge Univ. Press, New York.
- Prôno, E., J. Battaglia, V. Monteiller, J.-L. Got, and V. Ferrazzini (2009), P-wave velocity structure of Piton de la Fournaise volcano deduced from seismic data recorded between 1996 and 1999, *J. Volcanol. Geotherm. Res.*, *184*(1), 49–62.
- Rivet, D., F. Brenguier, D. Clarke, N. Shapiro, and A. Peltier (2014), Long-term dynamics of Piton de la Fournaise volcano from 13 years of seismic velocity change measurements and GPS observations, *J. Geophys. Res. Solid Earth*, *119*, doi:10.1029/2014JB011307.

- Roult, G., A. Peltier, B. Taisne, T. Staudacher, V. Ferrazzini, and A. di Muro (2012), A new comprehensive classification of the Piton de la Fournaise activity spanning the 1985-2010 period. Search and analysis of short-term precursors from a broad-band seismological station, *J. Volcanol. Geotherm. Res.*, *241*–242, 78–104.
- Schmid, A., J.-R. Grasso, D. Clarke, V. Ferrazzini, P. Bachèlery, and T. Staudacher (2012), Eruption forerunners from multiparameter monitoring and application for eruptions time predictability (Piton de la Fournaise), *J. Geophys. Res.*, *117*, B11203, doi:10.1029/2012JB009167.
- Shalev, E., and V. Lyakhovsky (2013), The processes controlling damage zone propagation induced by wellbore fluid injection, *Geophys. J. Int.*, *193*, 209–219.
- Staudacher, T., V. Ferrazzini, A. Peltier, P. Kowalski, P. Boissier, P. Catherine, F. Lauret, and F. Massin (2009), The April 2007 eruption and the Dolomieu crater collapse, two major events at Piton de la Fournaise (La Réunion Island, Indian Ocean), *J. Volcanol. Geotherm. Res.*, *184*(1–2), 126–137.
- Surono, P. J., et al. (2012), The 2010 explosive eruption of Java's Merapi volcano—A '100-year' event, *J. Volcanol. Geotherm. Res.*, *241*, 121–135.
- Tait, S., C. Jaupart, and S. Vergnolle (1989), Pressure, gas content and eruption periodicity of a shallow, crystallizing magma chamber, *Earth Planet. Sci. Lett.*, *92*, 107–123.
- Tarraga, M., R. Carniel, R. Ortiz, and A. Garcia (2008), The Failure Forecast Method: Review and application for the real-time detection of precursory patterns at reawakening volcanoes, *Dev. Volcanol.*, *10*, 447–469, doi:10.1016/S1871-644X(07)00013-7.
- Ventura, G., S. Vinciguerra, S. Moretti, P. Meredith, M. Heap, P. Baud, S. A. Shapiro, C. Dinske, and J. Kummerow (2010), Understanding slow deformation before dynamic failure, in *Geophysical Hazards*, edited by T. Beer, pp. 229–247, Springer, Netherlands.
- Voight, B. (1988), A method for prediction of volcanic eruptions, *Nature*, *332*, 125–130.
- Walsh, J. (1965), The effect of cracks on the uniaxial elastic compression of rock, *J. Geophys. Res.*, *70*, 399–411.
- Wells, D., and K. Coppersmith (1994), New empirical relationships among magnitude, rupture length, rupture width, rupture area, and surface displacement, *Bull. Seismol. Soc. Am.*, *84*(4), 974–1002.
- Woessner, J., and S. Wiemer (2005), Assessing the quality of earthquake catalogues: Estimating the magnitude of completeness and its uncertainty, *Bull. Seismol. Soc. Am.*, *95*(2), 684–698, doi:10.1785/0120040007.
- Zang, A., F. Wagner, S. Stanchits, C. Janssen, and G. Dresen (2000), Fracture process zone in granite, *J. Geophys. Res.*, *105*, 23,651–23,661.